First-Order Reversal Curve Probing of Spatially Resolved Polarization Switching Dynamics in Ferroelectric Nanocapacitors

Yunseok Kim,[†,*] Amit Kumar,[†] Oleg Ovchinnikov,[†] Stephen Jesse,[†] Hee Han,[‡] Daniel Pantel,[§] Ionela Vrejoiu,[§] Woo Lee,[‡] Dietrich Hesse,[§] Marin Alexe,[§] and Sergei V. Kalinin[†,*]

[†]The Center for Nanophase Materials Sciences, Oak Ridge National Laboratory, Oak Ridge, Tennessee 37831, United States, [‡]Korea Research Institute of Standards and Science (KRISS), Daejeon 305-340, Korea, and [§]Max Planck Institute of Microstructure Physics, D-06120 Halle (Saale), Germany

ABSTRACT

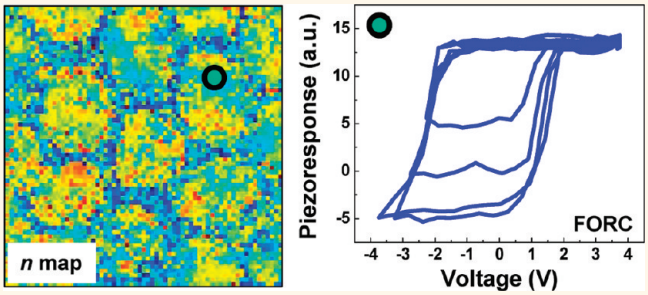

Spatially resolved polarization switching in ferroelectric nanocapacitors was studied on the sub-25 nm scale using the first-order reversal curve (FORC) method. The chosen capacitor geometry allows both high-veracity observation of the domain structure and mapping of polarization switching in a uniform field, synergistically combining microstructural observations and probing of uniform-field polarization responses as relevant to device operation. A classical Kolmogorov–Avrami–Ishibashi model has been adapted to the voltage domain, and the individual switching dynamics of the FORC response curves are well approximated by the adapted model. The comparison with microstructures suggests a strong spatial variability of the switching dynamics inside the nanocapacitors.

KEYWORDS: ferroelectric nanocapacitor · spatially resolved switching dynamics · PFM · BEPS · KAI · FORC

Polarization switching in ferroelectric materials underpins the functionality of ferroelectric-based data storage[1,2] and random access memory,[3,4] as well as emergent applications such as ferroelectric tunneling barriers,[5−8] domain wall electronics,[9−13] and ferroelectric gate transistors.[14,15] Hence, extensive efforts were aimed at understanding polarization switching dynamics in macro- and nanoscale systems. Classically, these phenomena are described by the Kolmogorov–Avrami–Ishibashi (KAI) model or similar statistical models often used to interpret the results of macroscopic polarization–electric field measurements.[16−22] However, the switching behavior in the ferroelectric materials varies locally due to the intrinsic randomness of the material.[21] Correspondingly, macroscopic electrical measurements are insufficient to describe *deterministic* switching dynamics on the level of single structural elements.

To establish the relationship between polarization switching and local microstructure and hence get insight into deterministic polarization switching mechanisms, local polarization switching in ferroelectric materials and devices has been extensively explored using hysteresis loop measurements in piezoresponse force microscopy (PFM) and switching spectroscopy PFM (SS-PFM).[23−31] On free surfaces, switching is localized within a small volume below the tip, and hence the process can be described using deterministic models.[32−35] These measurements can be similarly performed in capacitor structures, in which switching happens at defect sites[25,36,37] rather than at the tip location. In a few cases, domain growth and nucleation was observed, albeit at reduced resolution compared to tip-electrode PFM.[38] Recently, Wu *et al.* reported that the classical KAI model described well the switching dynamics in epitaxial $Pb(Zr,Ti)O_3$ (PZT) capacitor structures.[27] However, even though this imaging approach enables one to probe the switching dynamics over the entire area of the capacitor,[24,25,31,36] it does not provide information on the spatially resolved local switching dynamics within the capacitor. Moreover, this imaging approach does not provide information on the metastable polarization states since PFM imaging typically

* Address correspondence to kimy4@ornl.gov, sergei2@ornl.gov.

Received for review October 5, 2011 and accepted December 2, 2011.

Published online December 02, 2011
10.1021/nn203831h

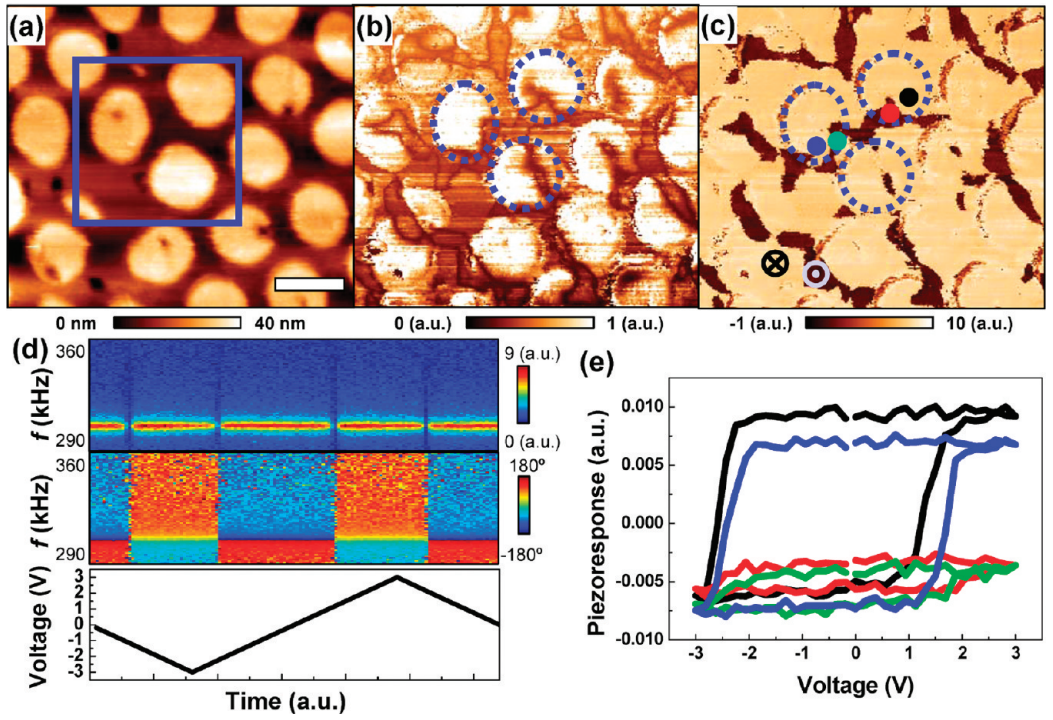

Figure 1. (a) Topography, (b) PFM amplitude, and (c) PFM phase of BFO nanocapacitors. Scale bar represents 400 nm. (d) BE amplitude (top) and phase (middle) spectra as a function of (bottom) varying bias voltage obtained from blue filled circle of panel c. (e) Piezoresponse hysteresis loops obtained from each color-filled circle of panel c: blue (green) and black (red) filled circles represent downward (upward) domain regions. The blue, green, red, and black filled circles are referred to as locations 1, 2, 3, and 4, respectively. The solid and dotted lines of panels a−c represent the scanned regions for BEPS and the capacitors, respectively.

takes a couple of minutes after applying the bias pulses.[30]

In larger capacitors, the origin of PFM imaging contrast still remains a challenge since the PFM signal itself can be affected by the bimorph-like response of the biased capacitor structure and its spatial resolution may not be enough to describe the nanoscale switching behavior over the entire capacitor.[39] The SS-PFM technique based on local hysteresis loop measurements provides further insight into the spatially resolved local switching properties.[26,28,29] However, the classical SS-PFM approach is limited by the fact that in hysteretic systems the knowledge of system response to one field history is insufficient to predict it for different histories and for hysteresis loops obtained for different bias windows.

Here, we use the first-order reversal curve (FORC) method based on SS-PFM to explore further spatially resolved local switching dynamics in $BiFeO_3$ (BFO) nanocapacitor structures. These structures allow the probing of local response to a uniform electric field, similar to the realistic operational conditions of ferroelectric devices. At the same time, these structures allow spatially resolved imaging of the domains structure. This approach hence allows one to explore the spatially resolved, history-dependent polarization dynamics in these systems and directly link it to the microstructure.

RESULTS AND DISCUSSION

Polarization Switching in Ferroelectric Nanostructures. As a model system, we have chosen (001) oriented film BFO nanocapacitors. These structures were prepared similarly to the PZT capacitor structures studied previously.[31,40] Pt nanoelectrodes with a diameter of 380 nm were deposited on a 90 nm thick BFO thin film. These structures offer an ideal model system since domain structures can be observed and switching dynamics can be studied through the thin Pt top electrodes. At the same time, the signal generation volume for top electrode PFM is much larger than that for the tip-electrode PFM as determined by capacitor size. Thus, they offer ideal model systems that can both allow a model for nanoscale switching dynamics of capacitor structures and provide correlation between polarization switching and the local microstructure.

As-grown domain structures of the BFO thin films show randomly distributed upward stripe domains inside a downward matrix.[41] It is well-known that there are eight polarization and three domain wall variants in epitaxial BFO films grown on $SrRuO_3$ (SRO)/$SrTiO_3$(STO)-(001).[10,42] Although the BFO thin films preferentially show a specific stripe shape of domains over the whole sample surface, the as-grown domain structures also show eight polarization variants with three different domain walls. Figure 1a−c shows typical topography and PFM images of BFO nanocapacitors. The as-grown

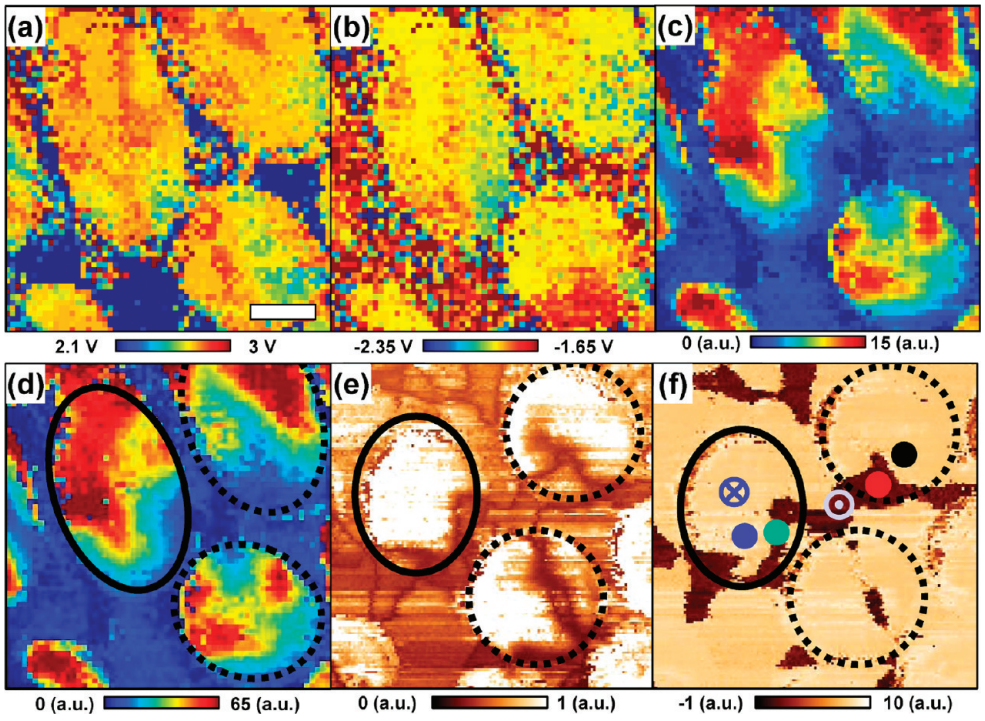

Figure 2. BEPS spatial maps of BFO nanocapacitors: (a) positive coercive voltage V_C^+, (b) negative coercive voltage V_C^-, (c) switchable polarization P_S, and (d) work of switching A_S. PFM (e) amplitude and (f) phase images of BFO nanocapacitors. The black lines of (d−f) mark the same capacitors in both PFM and BEPS images from the enlarged figures of Figure 1b,c. Scale bar is 200 nm.

domain structures underneath the capacitors can be well identified through Pt top electrodes and show randomly distributed upward stripe domains inside a downward matrix domain. The domain boundaries are continuous through the edges of the capacitors, suggesting that the deposition of the top electrode did not affect the domain structure of the BFO films, as shown in Figure 1b,c.

Spatially resolved switching behavior in the BFO nanocapacitors was explored using the band excitation (BE) switching spectroscopy PFM method (BEPS).[43] The bias-on steps in the waveform, comprising a sequence of dc bias pulses at regular intervals with magnitude following a triangular envelope, are used to switch polarization in the material, and a read-out is performed during bias-off steps (after each bias-on pulse) similar to typical hysteresis loop measurement.[29] For the BE method, a BE waveform centered at the contact resonance of the cantilever is applied to the tip during the bias-off steps. The individual hysteresis loops based on the BE method are acquired on a two-dimensional grid on the sample surface.[28,43,44]

An example of BE spectra obtained from location 1 of Figure 1c is presented in Figure 1d. Local switching events inside the capacitor are clearly observed as straight vertical lines where the amplitude becomes smaller than the noise floor and the phase changes by 180°. The frequency response curve of these data in Figure 1d is fitted using the simple harmonic oscillator model to yield amplitude, phase, quality factor, and resonant frequency.[43] The bias dependence of the piezoresponse, which is obtained from amplitude and phase, yields the local PFM hysteresis loops in Figure 1e.

Even though an entire capacitor was excited by applying the bias to the top electrode, the spatially varying piezoresponse was monitored at individual locations inside the capacitors, as shown in the hysteresis loops of Figure 1e. While the downward domain regions show clear switching events as a function of applied biases, some upward domain regions show incomplete polarization switching, evidence of the presence of pinned ferroelectric domains. As shown in Figure 1, the upward domains extend over long distances and even extend outside of the capacitors. Thus, they are able to act as pinning centers for switching as observed in the spatial maps of BEPS data (Figure 2). We argue that this pinning is due to the effect of domains extending outside of the capacitor region and hence unaffected by the applied electric field. This observation illustrates that the local switching behavior inside the capacitors can be monitored by a combination of domain imaging at different bias levels and BEPS mapping.

Spatially Resolved Mapping of Polarization Switching. To further explore the local switching properties, hysteresis loop measurements were performed over a dense 60 × 60 spatial point grid within the solid line box of Figure 1a.[45] Individual hysteresis loops were analyzed to extract switching coefficients.[29]

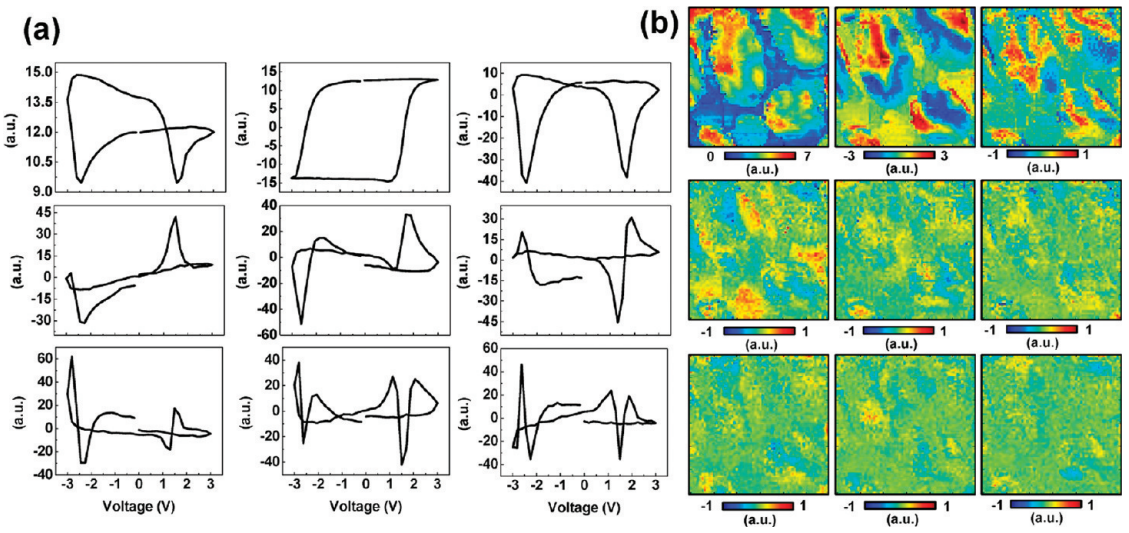

Figure 3. (a) First nine principal components from the PCA of BEPS images in Figure 2 and (b) their corresponding BEPS images. The image sequence in each figure is from left to right and then from top to bottom.

Local variations of ferroelectric switching coefficients,[44] including coercive voltage, switchable polarization, and work of switching, are shown in Figure 2. The spatial resolution of Figure 2 is better than 20 nm, which is the highest reported to date for SS-PFM of capacitor structures, and allows the exploration of the spatially resolved switching behavior inside the capacitors. The spatial maps of the switchable polarization and work of switching show highly resolved images with large spatial distributions. The variability can be as large as 27−38% for switchable polarization and work of switching within a capacitor (Figure 2).

Intriguingly, the local variations show a strong correlation with the pre-existing domain structures underlying the nanocapacitors. The downward domain regions show higher switchable polarization, positive coercive voltage, and work of switching and lower negative coercive voltage. The lower switchable polarization and work of switching of upward domain regions are relevant to the incomplete polarization switching, as seen in Figure 1e. While the piezoresponse hysteresis loops of Figure 1e only provide discrete switching information of a few different points, the highly resolved spatial BEPS maps of Figure 2c,d allow the exploration of the spatial change in the switching properties; that is, both the switchable polarization and the work of switching gradually change from upward to downward domains, which is probably related to the domain wall motion of the pre-existing domain wall. Higher positive and lower negative coercive voltages of downward domain regions indicate that downward (upward) domain regions have a positive (negative) bias shift. In this situation, nucleation under the positive (negative) biases primarily starts from upward (downward) domain regions, domain boundaries between upward and downward domain regions, and/or capacitor boundaries near the upward (downward) domain regions; see bright blue (red) regions of Figure 2a (2b).

Spatial distributions of the switching properties were also found from principal component analysis (PCA), which allows the identification of relevant components and corresponding component spectra of the data set.[46] While direct interpretation of PCA components in terms of physical mechanisms is typically impossible since they are statistically defined, this approach allows optimal visualization of variability of the response. Furthermore, in some cases, semiqualitative interpretation of PCA decomposition data can be achieved based on the shape of corresponding eigenvectors.[47] For instance, the components 1 and 2 of Figure 3 can be roughly identified as corresponding to vertical shift and area under the hysteresis loops and show the strongest spatial variation. The third component is effectively the loop width, whereas the fourth is imprint. Components 5 and above represent the variability of the hysteresis loops between successive cycles at the same point. Note that these components are very weak and show largely random spatial distribution. Overall, PCA analysis suggests that the variability of the hysteresis loop is primarily determined by four primary parameters; that is, they can be captured well by SS-PFM parameter maps.

First-Order Reversal Curve Measurements. Quantification of the polarization switching in material requires knowledge of the fraction of switched material *versus* the applied voltage. Ideally, this information is encoded in the measured PFM signal. However, we note that contributions of electrostatic interactions and intrinsic piezoelectric nonlinearity, while minimized in the off-field PFM measurements, cannot be completely excluded. Furthermore, a single hysteresis loop is insufficient to fully study the polarization switching; that is, the signal evolution in the minor loop can

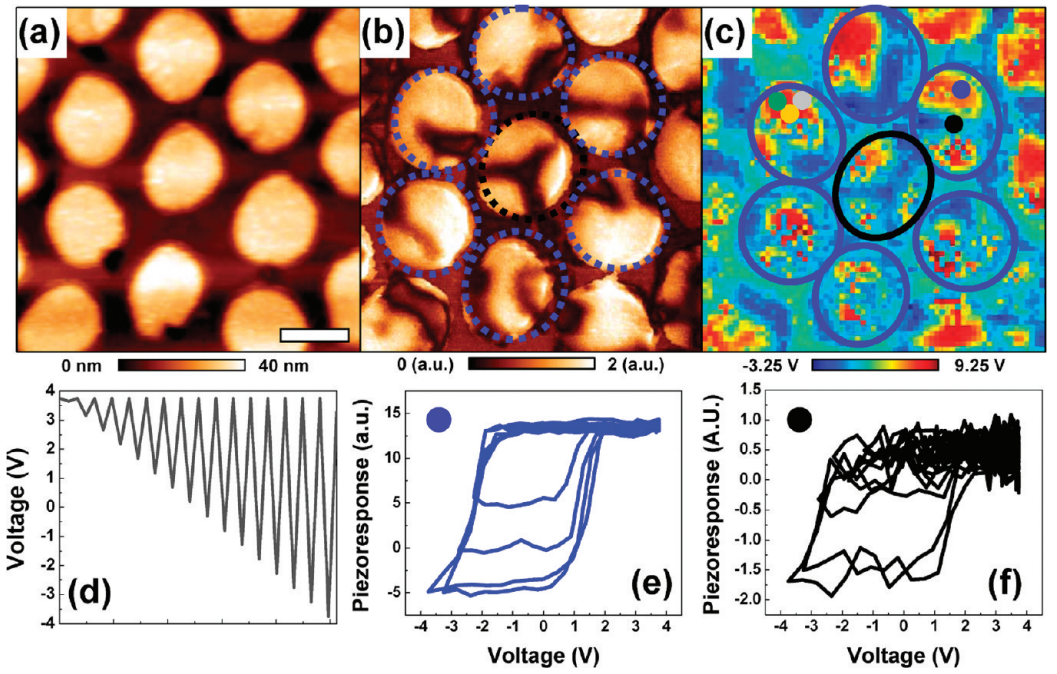

Figure 4. (a) Topography and (b) PFM amplitude images of BFO nanocapacitors for FORC-BEPS measurements. (c) Sum of piezoresponse and (d) bias voltage sweep for FORC-BEPS measurements. (e,f) Each FORC was measured at the (e) blue and (f) black filled circles of panel c, respectively. (The other FORCs of green, yellow, and gray filled circles are presented in Figure 6.) Black and blue lines mark the present capacitors. Scale bar corresponds to 320 nm.

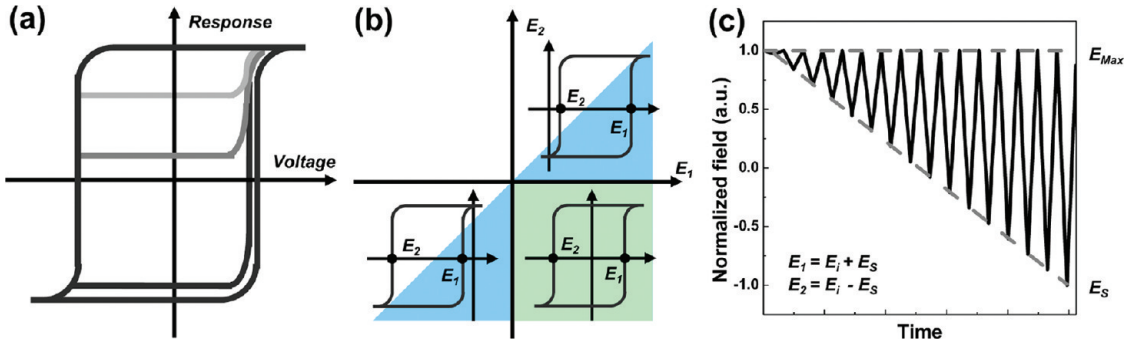

Figure 5. Schematics of (a) signal evolution in the first minor loops with multiple pathways (each loop corresponds to a first minor loop) and (b) Preisach plane and the segments probed in on-field (bright blue) and off-field (bright green) measurements. (b) Instant field (E_i) evolution along time and stopping field (E_S) for each loop.

proceed along multiple pathways that are not known *a priori* (see Figures 5a and 6). To probe polarization switching mechanisms further and explore the multiple remnant states dependent on field history, FORC[47−49] measurements with the BE approach (FORC-BEPS) are carried out.

The principle of FORC-BEPS measurements is illustrated in Figure 4d. A triangular wave with progressively increasing relative amplitude defines the envelope of the FORC waveform (here, 16 hysteresis loops). The wave is modulated by high-frequency (2 ms) rectangular pulses. From the comparison between panels b and c of Figure 4, it was found that the FORC results also strongly depend on the pre-existing domain structures. Figure 4e,f shows individual FORCs. While some upward domain regions show incomplete switching similar to BEPS (Figure 4f), all downward domain regions show complete switching (Figure 4e). Intriguingly, all of the forward segments coincide, which shows reproducibility and no time drift (Figure 4e). We note that all loops have horizontal reversal curves, as can be expected for off-field measurements in the absence of slow relaxation kinetics. This is further confirmed by direct relaxation measurements (Figure S1 of the Supporting Information), indicating that there was no significant relaxation on the switched states of BEPS up to 300 ms.

We further analyze FORC data using the Preisach model.[47−49] In this, a system is represented as a superposition of linear bistable elements (hysterons) characterized by upper (E_2) and lower (E_1) switching fields (Figure 5b,c). The density of hysterons as a function of

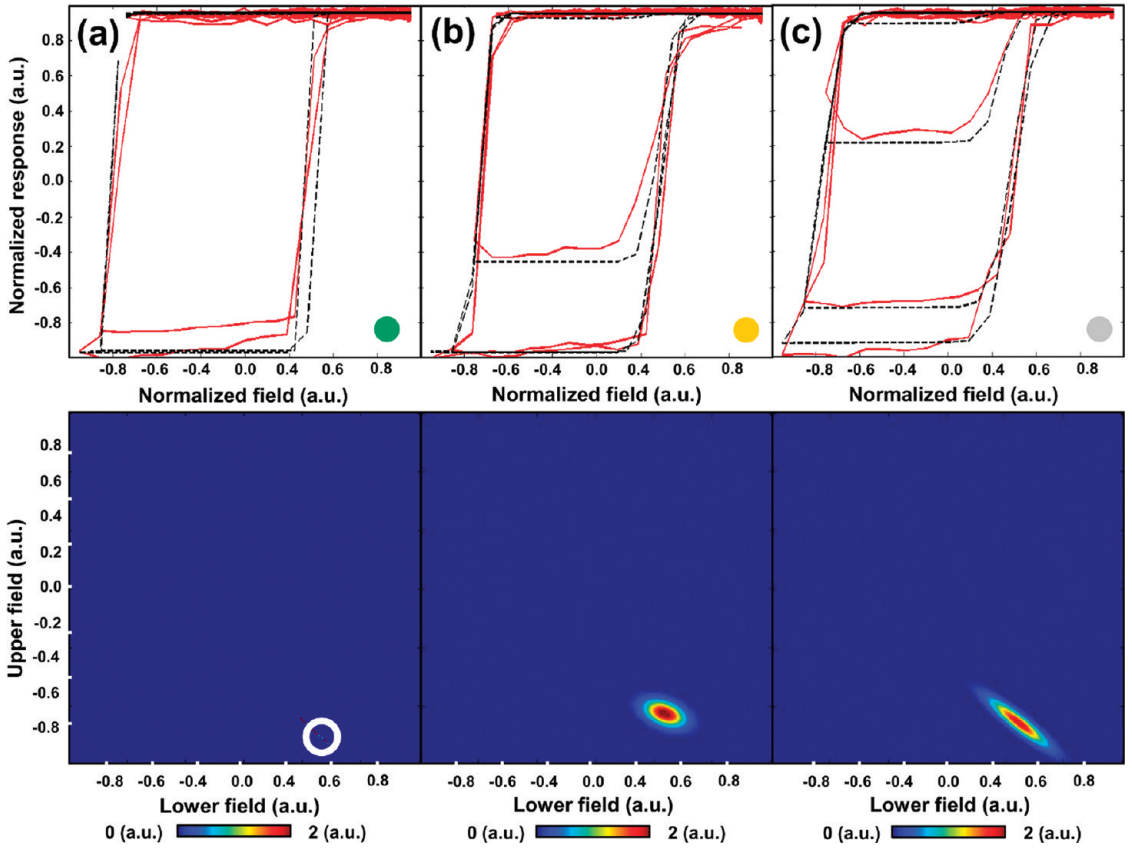

Figure 6. Normalized FORCs (red lines) and their Gaussian fitted curves (black dashed lines) (top) and Preisach density (bottom) at the positions of (a) green, (b) yellow, and (c) gray filled circles of Figure 4. The white unfilled circle in panel a shows the location of the delta-function-type feature.

switching fields describes the response of the system for an arbitrary field history. The corresponding Preisach density can be determined from FORC data.

As shown in Figure 6, FORCs were obtained from three different downward domain regions within the same capacitor, and each FORC shows different switching behavior even inside the downward domain region. The Preisach density of Figure 6 simply presents the population map of the switching fields. For instance, the Preisach density of Figure 6c has a slanted elliptical shape, which means that the switching fields of diagonal axis are laterally more diffused. The different FORCs and their corresponding Preisach density are relevant to the switching procedures inside the capacitor. The Preisach density in Figure 6a shows a single delta-function-type feature, which means that there is no disorder and all of the switching events uniformly happen at a specific voltage. Note that the width of the Gaussian peak in the Preisach density is very narrow, and spatial variability is primarily related to the variation of the corresponding critical fields.

Switching Mechanisms in KAI Formalism. In the present FORC-BEPS measurements, we use a one directional bias sweep, in which the bias sweep is from positive to negative. For the switching dynamics studies, switching pulse trains of different pulse conditions with the same set pulses are applied and the switching is evaluated by subsequent PFM imaging or electrical measurements at each step.[17,30] Here, each envelope of the waveform shows the triangular wave from a fixed maximum positive amplitude to a progressively increasing relative amplitude toward the maximum negative amplitude. Hence, the maximum positive bias (progressively increasing relative amplitude) can be regarded as a set (switching) pulse of the typical switching experiments. This bias sweep allows us to explore further the nucleation and domain growth dynamics under negative directional biases.

As mentioned above, one of the drawbacks of the imaging approach is the unstable part of the switched regions. However, the present FORC-BEPS approach collects the polarization switching information just after applying the bias pulse, which means that the unstable part of the switched regions can be minimized (see Figure S1 in Supporting Information).

For ferroic materials, polarization switching dynamics are classically described by the Kolmogorov–Avrami–Ishibashi (KAI) model[16,17]

$$\frac{\Delta P(t)}{P_S} = P(t) = 1 - \exp\left[-\left(\frac{t}{\tau}\right)^n\right] \qquad (1)$$

where $\Delta P(t)$, P_S, $P(t)$, n, and τ are the switched polarization, the saturation polarization (here, the switchable polarization), the volume fraction of the switched polarization at time t, the geometric dimension of the domain growth, and the characteristic switching time, respectively. The KAI approach is expected to be applicable for statistically well averaged situations and gives us the dimensionality of the process. For tip-electrode PFM on conventional (nonrelaxor) ferroelectrics, the KAI model cannot be expected to be applicable due to the presence of a single nucleation center and a nonuniform field distribution. However, once the top electrodes are sufficiently large, the field (within the capacitor) is almost uniform and the KAI can be applicable for top electrode PFM.[27] Indeed, the KAI model was well described by switching dynamics using a step-by-step PFM approach based on top electrode PFM.[27]

For the PFM imaging approaches such as step-by-step PFM,[24,25,27,31] the switching information is collected from the contrast change in the PFM image over the entire area of the capacitor. On the contrary, the present FORC-BEPS approach for the switching dynamics is based on the collection of local piezoresponse at individual measuring points (not from images) within the nanocapacitors. Although the bias pulse sweep is applied to the entire nanocapacitor (global excitation), the piezoresponse, raised from the local switching event, can be only collected near the tip position (local measurement). It has contributions from directly below the tip and adjacent regions. Hence, this approach is a "hybrid" of local and nonlocal cases. Thus, using the FORC-BEPS approach, the spatial distribution of the KAI coefficients, such as the geometric dimension n, can be obtained and provide insight into the local switching dynamics. For instance, if the KAI coefficients are the same everywhere, this means that multiple (almost spatially uniform) defect centers control the switching in a capacitor. However, if these parameters change strongly with location, of interest will be the variability inside a capacitor and the correlation of the KAI parameters with the local microstructure and a comparison of the average local coefficients with the macroscopic ones.

Typically, the KAI model describes the domain growth process in the time domain. However, this time domain is very inefficient to explore domain switching dynamics because it takes many orders of magnitude in time. On the other hand, it is well-known that the characteristic switching time τ exhibits a strong dependence on the local voltage bias which can be found from both the empirical law of electrical measurements[17,50,51] and creep motion of PFM measurements[52]

$$\tau(V) = \tau_0 \exp\left(\frac{V_0}{V}\right) \quad (2)$$

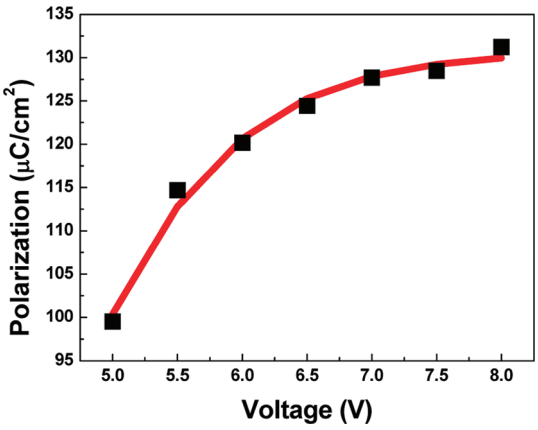

Figure 7. Switched polarization (black symbols) from switching current as a function of voltage. The solid line shows the fitting result using the adapted KAI model.

where τ_0 is the characteristic switching time constant and V_0 is the activation voltage. Li *et al.* reported an adapted KAI model combined with the above relationship to describe a frequency-dependent coercive field in ferroelectric thin films.[53] Using eq 2, the KAI model can also be adapted to be more efficient to explore polarization switching dynamics. Thus, the adapted KAI model can be described as follows:

$$\frac{\Delta P(t, V)}{P_S} = 1 - \exp\left[-\left(\frac{t}{\tau_0}\right)^n \exp\left(-\frac{nV_0}{V}\right)\right] \quad (3)$$

Considering the absolute value (instead of the volume fraction) of $\Delta P(t,V)$ with constant time t, eq 3 can be rewritten as

$$\Delta P(V) = P_S\left\{1 - \exp\left[-\left(\frac{t}{\tau_0}\right)^n \exp\left(-\frac{nV_0}{V}\right)\right]\right\} \quad (4)$$

In order to explore the validity of the adapted KAI model of eq 4 for macroscopic systems, polarization switching based on macroscopic electrical measurements was performed on a capacitor of an area of 750 μm^2 prepared on 300 nm thick (001) oriented BFO films using bias pulse trains, which is similar to ref 18.[18,54] The detailed measurements can be found elsewhere.[54] Since we assume that the activation voltage V_0 is constant in eq 2, the polarization switching data were only collected from the constant activation voltage regime (high voltage regime of Figure 3c in ref 54). The fit of Figure 7 shows a good approximation and the obtained values (the switchable polarization P_S = 131.7 $\mu C/cm^2$, the geometric dimension n = 1.1, and the activation voltage V_0 = 15 V) are rather similar to those of ref 54. This indicates the validity of the adapted KAI model.

From the FORC data, the work of switching of the ith loop $\Delta A_{S,i}$ can be approximately rewritten as $(-V_{C,n} + N_p)\Delta P_i$, where $V_{C,n}$, N_p, and ΔP_i are negative coercive voltage, positive nucleation voltage, and

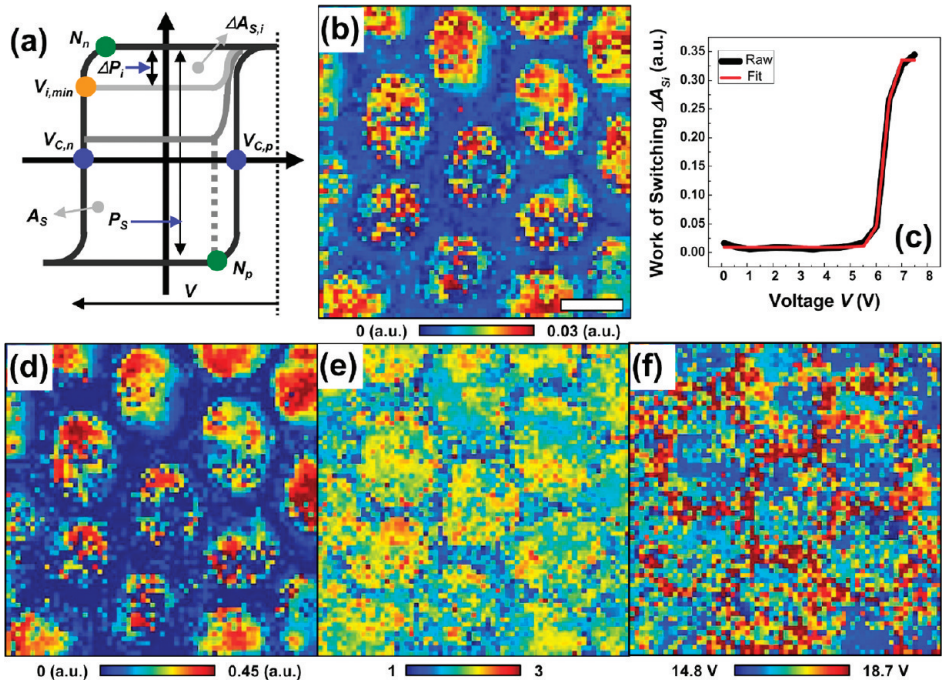

Figure 8. (a) Schematic of FORCs. (b) Switchable polarization P_S of the 16th loop of FORC from Figure 4. (c) Raw (black line) and fitted (red line) work of switching curve as a function of the voltage difference V between the positive maximum and the local minimum voltage $V_{i,min}$. Spatial maps of KAI coefficients: (d) A_S, (e) n, and (f) V_0 of work of switching curve. Scale bar corresponds to 320 nm.

accumulated switched polarization of the ith loop, respectively (see Figure 8a). If we additionally assume that ΔP_i is equal to $\Delta P_{i,min}$, which is the instantaneous switched polarization generated at the local minimum bias pulse $V_{i,min}$ of the ith loop, the work of switching of the ith loop $\Delta A_{S,i}$ can be linearly proportional to the instantaneous switched polarization $\Delta P_{i,min}$. In this situation, the switchable polarization P_S can be also replaced by the work of switching A_S since they also have a linear relationship. Hence, eq 4 can be rewritten again as

$$\Delta A_S(V) = A_S\left\{1 - \exp\left[-\left(\frac{t}{\tau_0}\right)^n \exp\left(-\frac{nV_0}{V}\right)\right]\right\} + A_{S,offset} \quad (5)$$

where $\Delta A_S(V)$ and $A_{S,offset}$ are the work of switching for the switched polarization and the noise offset, respectively. Here, the noise offset was introduced to have a better fitting; however, the noise offset is nearly zero (the mean value of the noise offset over the whole measured area is 8.9×10^{-3}). This replacement procedure allows a more reliable approach for the analysis of switching dynamics since the area data of the work of switching obviously are less noisy than the single point data of the switched polarization.

To describe the switching dynamics of the BFO nanocapacitors, the work of switching of the ith loop $\Delta A_{S,i}$ was extracted from each FORC and was presented as a function of the voltage difference V between the positive maximum (here, +3.75 V) and the local minimum voltage $V_{i,min}$ as shown in Figure 8c. Even though some of the points show an inconsistency at the beginning or ending stages which might be relevant to local nucleation[31] and/or variable activation voltages,[54] the fit results primarily show a good approximation (red line of Figure 8c). Figure 8d–f shows KAI coefficients of A_S, n, and V_0, respectively. The work of switching A_S map of Figure 8d is very similar to the switchable polarization P_S map of the 16th loop of FORC (Figure 8b). This shows the validity of the above assumption on the linear relationship between the switchable polarization P_S and the work of switching A_S.

The dotted blue pixels within the capacitors of Figure 8b,d are relevant to the incomplete switching of upward domain regions. The geometric dimension n of the domain wall motion was primarily around 2, which shows that the domain wall geometry inside the capacitors had a two-dimensional domain growth, and some of the n values near the domain and capacitor boundaries are close to 3, which is probably related to the nucleation sites. The activation voltage V_0 also shows a spatial distribution inside the capacitors and is in the range between 15 and 20 V, which can be rewritten as an actual activation electric field between 1.25 and 1.8×10^8 V/m. The obtained field is in the similar range of the negative activation electric field of BFO thin films.[54,55] The proper values from the adapted KAI model clearly show that the present model describes well the polarization switching dynamics of BFO nanocapacitors.

SUMMARY

In summary, we have investigated spatially resolved polarization switching processes of BFO nanocapacitors using the SS-PFM technique. The spatial maps of the switching coefficients using highly resolved BEPS measurements, which possess the highest resolution to date, show that the switching properties depend on pre-existing domain patterns. The spatial maps and the Preisach density of the FORCs also reveal that the individual polarization switching inside the nanocapacitors depends on the pre-existing domain patterns. In order to analyze the switching behavior of the FORCs in BFO nanocapacitors, the classical KAI model has been adapted to the voltage domain. The polarization switching dynamics of the FORCs are well approximated by the adapted KAI model. The KAI coefficients show spatial distributions inside the capacitors and reveal that domain wall motion inside a capacitor primarily undergoes two-dimensional domain growth. The proper obtained values from the adapted KAI model shows that the present model describes well the polarization switching dynamics of BFO nanocapacitors. The results both show the spatially resolved nanoscale switching dynamics of capacitor structures on the sub-25 nm scale and provide a correlation between polarization switching and the local microstructure. Notably, the resolution (about 600 nm^2) on the local switching dynamics is remarkably higher than that of the previous reports which corresponded to at least about 4000 nm^2.[2,24,25,27,31] This approach allows one to explore spatially resolved switching dynamics in the nanoscale range and will enable further insight into the control of device functionalities to achieve a high memory density.

METHODS

Materials. A 90 nm thick (001) oriented epitaxial BFO thin film was prepared by pulsed laser deposition on SRO/STO substrate. Twenty-five nanometer thick Pt was deposited on top of the thin films through ultrathin anodic aluminum oxide (AAO) masks by electron beam evaporation. After removing the AAO mask, the film-type Pt/BFO/SRO nanocapacitors with a diameter of around 380 nm were successfully obtained. The detailed fabrication information of the thin films and AAO masks can be found elsewhere.[31,40,41,56] For microscopic electrical measurements, 300 nm thick (001) oriented epitaxial BFO films were grown on SRO/STO substrates. An epitaxial SRO top electrode with an area of 750 μm^2 was deposited on the films. The details on the growth process and the electrical measurements are published elsewhere.[54]

Measurements. Atomic force microscopy studies were performed with a commercial system (Asylum Cypher) additionally equipped with a Labview/Matlab based BE controller. PFM was carried out with ~300 kHz of 0.4 V_{pp} ac bias applied to a Pt/Cr-coated probe (Budget sensors Multi75E-G). BEPS and FORC-BEPS were performed with 280−400 kHz of 0.4 V_{pp} BE signal applied to the conductive probe.

Acknowledgment. This research was supported (S.V.K., Y.K.) by the U.S. Department of Energy, Basic Energy Sciences, Materials Sciences and Engineering Division and partially performed at the Center for Nanophase Materials Sciences (S.V.K.), a DOE-BES user facility. The work of Max Planck Institute of Microstructure Physics was supported by German Science Foundation (DFG) *via* SFB 762.

Supporting Information Available: Relaxation of the BEPS and an application of the adapted KAI model for the spatial maps of fitting parameters obtained from eq 4. This material is available free of charge *via* the Internet at http://pubs.acs.org.

REFERENCES AND NOTES

1. Ahn, C. H.; Tybell, T.; Antognazza, L.; Char, K.; Hammond, R. H.; Beasley, M. R.; Fischer, Ø.; Triscone, J.-M. Nonvolatile Electronic Writing of Epitaxial $Pb(Zr_{0.52}Ti_{0.48})O_3/SrRuO_3$ Heterostructures. *Science* **1997**, *276*, 1100–1103.
2. Tanaka, K.; Kurihashi, Y.; Uda, T.; Daimon, Y.; Odagawa, N.; Hirose, R.; Hiranaga, Y.; Cho, Y. Scanning Nonlinear Dielectric Microscopy Nano-Science and Technology for Next Generation High Density Ferroelectric Data Storage. *Jpn. J. Appl. Phys.* **2008**, *47*, 3311–3325.
3. Scott, J. F. *Ferroelectric Memories*; Springer: Heidelberg, 2000.
4. Waser, R.; Bottger, U.; Tiedke, S. *Polar Oxides: Properties, Characterization and Imaging*; John Wiley & Sons Inc.: New York, 2004.
5. Kohlstedt, H.; Pertsev, N. A.; Rodríguez Contreras, J.; Waser, R. Theoretical Current−Voltage Characteristics of Ferroelectric Tunnel Junctions. *Phys. Rev. B* **2005**, *72*, 125341.
6. Maksymovych, P.; Jesse, S.; Yu, P.; Ramesh, R.; Baddorf, A. P.; Kalinin, S. V. Polarization Control of Electron Tunneling into Ferroelectric Surfaces. *Science* **2009**, *324*, 1421–1425.
7. Garcia, V.; Bibes, M.; Bocher, L.; Valencia, S.; Kronast, F.; Crassous, A.; Moya, X.; Enouz-Vedrenne, S.; Gloter, A.; Imhoff, D.; *et al.* Ferroelectric Control of Spin Polarization. *Science* **2010**, *327*, 1106–1110.
8. Pantel, D.; Goetze, S.; Hesse, D.; Alexe, M. Room-Temperature Ferroelectric Resistive Switching in Ultrathin $Pb(Zr_{0.2}Ti_{0.8})O_3$ Films. *ACS Nano* **2011**, *5*, 6032–6038.
9. Maksymovych, P.; Seidel, J.; Chu, Y. H.; Wu, P.; Baddorf, A. P.; Chen, L.-Q.; Kalinin, S. V.; Ramesh, R. Dynamic Conductivity of Ferroelectric Domain Walls in $BiFeO_3$. *Nano Lett.* **2011**, *11*, 1906–1912.
10. Seidel, J.; Martin, L. W.; He, Q.; Zhan, Q.; Chu, Y.-H.; Rother, A.; Hawkridge, M. E.; Maksymovych, P.; Yu, P.; Gajek, M.; *et al.* Conduction at Domain Walls in Oxide Multiferroics. *Nat. Mater.* **2009**, *8*, 229–234.
11. Morozovska, A. N.; Eliseev, E. A.; Bravina, S. L.; Kalinin, S. V. Resolution-Function Theory in Piezoresponse Force Microscopy: Wall Imaging, Spectroscopy, and Lateral Resolution. *Phys. Rev. B* **2007**, *75*, 174109.
12. Gureev, M. Y.; Tagantsev, A. K.; Setter, N. Head-to-Head and Tail-to-Tail 180° Domain Walls in an Isolated Ferroelectric. *Phys. Rev. B* **2011**, *83*, 184104.
13. Kim, Y.; Alexe, M.; Salje, E. K. H. Nanoscale Properties of Thin Twin Walls and Surface Layers in Piezoelectric WO_{3-x}. *Appl. Phys. Lett.* **2010**, *96*, 032904.
14. Mathews, S.; Ramesh, R.; Venkatesan, T.; Benedetto, J. Ferroelectric Field Effect Transistor Based on Epitaxial Perovskite Heterostructures. *Science* **1997**, *276*, 238–240.
15. Takahashi, K. S.; Gabay, M.; Jaccard, D.; Shibuya, K.; Ohnishi, T.; Lippmaa, M.; Triscone, J.-M. Local Switching of Two-Dimensional Superconductivity Using the Ferroelectric Field Effect. *Nature* **2006**, *441*, 195–198.
16. Avrami, M. Kinetics of Phase Change. II Transformation-Time Relations for Random Distribution of Nuclei. *J. Chem. Phys.* **1940**, *8*, 212.
17. Ishibashi, Y.; Takagi, Y. Note on Ferroelectric Domain Switching. *J. Phys. Soc. Jpn.* **1971**, *31*, 506–510.

18. Tagantsev, A. K.; Stolichnov, I.; Setter, N. Non-Kolmogorov–Avrami Switching Kinetics in Ferroelectric Thin Films. *Phy. Rev. B* **2002**, *66*, 214109.
19. Dawber, M.; Gruverman, A.; Scott, J. Skyrmion Model of Nano-Domain Nucleation in Ferroelectrics and Ferromagnets. *J. Phys.: Condens. Matter* **2006**, *18*, L71.
20. Jo, J. Y.; Han, H. S.; Yoon, J. G.; Song, T. K.; Kim, S. H.; Noh, T. W. Domain Switching Kinetics in Disordered Ferroelectric Thin Films. *Phys. Rev. Lett.* **2007**, *99*, 267602.
21. Zhukov, S.; Genenko, Y. A.; von Seggern, H. Experimental and Theoretical Investigation on Polarization Reversal in Unfatigued Lead-Zirconate-Titanate Ceramic. *J. Appl. Phys.* **2010**, *108*, 014106.
22. Zhukov, S.; Genenko, Y. A.; Hirsch, O.; Glaum, J.; Granzow, T.; von Seggern, H. Dynamics of Polarization Reversal in Virgin and Fatigued Ferroelectric Ceramics by Inhomogeneous Field Mechanism. *Phys. Rev. B* **2010**, *82*, 014109.
23. Hong, S.; Colla, E. L.; Kim, E.; Taylor, D. V.; Tagantsev, A. K.; Muralt, P.; No, K.; Setter, N. High Resolution Study of Domain Nucleation and Growth during Polarization Switching in $Pb(Zr,Ti)O_3$ Ferroelectric Thin Film Capacitors. *J. Appl. Phys.* **1999**, *86*, 607.
24. Gruverman, A.; Rodriguez, B. J.; Dehoff, C.; Waldrep, J. D.; Kingon, A. I.; Nemanich, R. J.; Cross, J. S. Direct Studies of Domain Switching Dynamics in Thin Film Ferroelectric Capacitors. *Appl. Phys. Lett.* **2005**, *87*, 082902.
25. Kim, D. J.; Jo, J. Y.; Kim, T. H.; Yang, S. M.; Chen, B.; Kim, Y. S.; Noh, T. W. Observation of Inhomogeneous Domain Nucleation in Epitaxial $Pb(Zr,Ti)O_3$ Capacitors. *Appl. Phys. Lett.* **2007**, *91*, 132903.
26. Wu, D.; Kunishima, I.; Roberts, S.; Gruverman, A. Spatial Variations in Local Switching Parameters of Ferroelectric Random Access Memory Capacitors. *Appl. Phys. Lett.* **2009**, *95*, 092901.
27. Wu, D.; Vrejoiu, I.; Alexe, M.; Gruverman, A. Anisotropy of Domain Growth in Epitaxial Ferroelectric Capacitors. *Appl. Phys. Lett.* **2010**, *96*, 112903.
28. Sharma, P.; Reece, T. J.; Ducharme, S.; Gruverman, A. High-Resolution Studies of Domain Switching Behavior in Nanostructured Ferroelectric Polymers. *Nano Lett.* **2011**, *11*, 1970–1975.
29. Jesse, S.; Rodriguez, B. J.; Choudhury, S.; Baddorf, A. P.; Vrejoiu, I.; Hesse, D.; Alexe, M.; Eliseev, E. A.; Morozovska, A. N.; Zhang, J.; Chen, L.-Q.; Kalinin, S. V. Direct Imaging of the Spatial and Energy Distribution of Nucleation Centres in Ferroelectric Materials. *Nat. Mater.* **2008**, *7*, 209–215.
30. Yang, S. M.; Yoon, J.-G.; Noh, T. W. Nanoscale Studies of Defect-Mediated Polarization Switching Dynamics in Ferroelectric Thin Film Capacitors. *Curr. Appl. Phys.* **2011**, *11*, 1111–1125.
31. Kim, Y.; Han, H.; Lee, W.; Baik, S.; Hesse, D.; Alexe, M. Non-Kolmogorov–Avrami–Ishibashi Switching Dynamics in Nanoscale Ferroelectric Capacitors. *Nano Lett.* **2010**, *10*, 1266–1270.
32. Morozovska, A. N.; Svechnikov, S. V.; Eliseev, E. A.; Jesse, E.; Rodriguez, B. J.; Kalinin, S. V. The Piezoresponse Force Microscopy of Surface Layers and Thin Films: Effective Response and Resolution Function. *J. Appl. Phys.* **2007**, *102*, 114108.
33. Morozovska, A. N.; Svechnikov, S. V.; Eliseev, E. A.; Rodriguez, B. J.; Jesse, S.; Kalinin, S. V. Local Polarization Switching in the Presence of Surface-Charged Defects: Microscopic Mechanisms and Piezoresponse Force Spectroscopy Observations. *Phys. Rev. B* **2008**, *78*, 054101.
34. Emelyanov, A. Y. Coherent Ferroelectric Switching by Atomic Force Microscopy. *Phys. Rev. B* **2005**, *71*, 132102.
35. Molotskii, M. Generation of Ferroelectric Domains in Atomic Force Microscope. *J. Appl. Phys.* **2003**, *93*, 6234.
36. Gruverman, A.; Wu, D.; Scott, J. F. Piezoresponse Force Microscopy Studies of Switching Behavior of Ferroelectric Capacitors on a 100-ns Time Scale. *Phys. Rev. Lett.* **2008**, *100*, 097601.
37. Colla, E. L.; Stolichnov, I.; Bradely, P. E.; Setter, N. Direct Observation of Inversely Polarized Frozen Nanodomains in Fatigued Ferroelectric Memory Capacitors. *Appl. Phys. Lett.* **2003**, *82*, 1604.
38. Kalinin, S. V.; Rodriguez, B. J.; Kim, S.-H.; Hong, S.-K.; Gruverman, A.; Eliseev, E. A. Imaging Mechanism of Piezoresponse Force Microscopy in Capacitor Structures. *Appl. Phys. Lett.* **2008**, *92*, 152906.
39. Bintachitt, P.; Trolier-McKinstry, S.; Seal, K.; Jesse, S.; Kalinin, S. V. Switching Spectroscopy Piezoresponse Force Microscopy of Polycrystalline Capacitor Structures. *Appl. Phys. Lett.* **2006**, *94*, 042906.
40. Kim, Y.; Han, H.; Rodriguez, B. J.; Vrejoiu, I.; Lee, W.; Baik, S.; Hesse, D.; Alexe, M. Individual Switching of Film-Based Nanoscale Epitaxial Ferroelectric Capacitors. *J. Appl. Phys.* **2010**, *108*, 042005.
41. Kim, Y.; Vrejoiu, I.; Hesse, D.; Alexe, M. Reversible Plasma Switching in Epitaxial $BiFeO_3$ Thin Films. *Appl. Phys. Lett.* **2010**, *96*, 202902.
42. Zavaliche, F.; Das, R. R.; Kim, D. M.; Eom, C. B.; Yang, S. Y.; Shafer, P.; Ramesh, R. Ferroelectric Domain Structure in Epitaxial $BiFeO_3$ Films. *Appl. Phys. Lett.* **2005**, *87*, 182912.
43. Jesse, S.; Maksymovych, P.; Kalinin, S. V. Rapid Multidimensional Data Acquisition in Scanning Probe Microscopy Applied to Local Polarization Dynamics and Voltage Dependent Contact Mechanics. *Appl. Phys. Lett.* **2008**, *93*, 112903.
44. Jesse, S.; Kalinin, S. V.; Proksch, R.; Baddorf, A. P.; Rodriguez, B. J. The Band Excitation Method in Scanning Probe Microscopy for Rapid Mapping of Energy Dissipation on the Nanoscale. *Nanotechnology* **2007**, *18*, 435503.
45. Note that, since BEPS measurements took about 3 h for the small area, there was a thermal drift which show the elongated features in the images.
46. Jesse, S.; Kalinin, S. V. Principal Component and Spatial Correlation Analysis of Spectroscopic-Imaging Data in Scanning Probe Microscopy. *Nanotechnology* **2009**, *20*, 085714.
47. Guo, S.; Ovchinnikov, O. S.; Curtis, M. E.; Johnson, M. B.; Jesse, S.; Kalinin, S. V. Spatially Resolved Probing of Preisach Density in Polycrystalline Ferroelectric Thin Films. *J. Appl. Phys.* **2010**, *108*, 084103.
48. Preisach, F. Uber die Magnetische Nachwirkung. *Z. Phys.* **1935**, *94*, 277–302.
49. Ovchinnikov, O.; Jesse, S.; Guo, S.; Seal, K.; Bintachitt, P.; Fujii, I.; Trolier-Mckinstry, S.; Kalinin, S. V. Local Measurements of Preisach Density in Polycrystalline Ferroelectric Capacitors Using Piezoresponse Force Spectroscopy. *Appl. Phys. Lett.* **2010**, *96*, 112906.
50. Merz, W. J. Domain Formation and Domain Wall Motions in Ferroelectric $BaTiO_3$ Single Crystals. *Phys. Rev.* **1954**, *95*, 690–698.
51. Wieder, H. H. Model for Switching and Polarization Reversal in Colemanite. *J. Appl. Phys.* **1960**, *31*, 180.
52. Tybell, T.; Paruch, P.; Giamarchi, T.; Triscone, J.-M. Domain Wall Creep in Epitaxial Ferroelectric $Pb(Zr_{0.2}Ti_{0.8})O_3$ Thin Films. *Phys. Rev. Lett.* **2002**, *89*, 097601.
53. Li, W.; Chen, Z.; Auciello, O. Calculation of Frequency-Dependent Coercive Field Based on the Investigation of Intrinsic Switching Kinetics of Strained $Pb(Zr_{0.2}Ti_{0.8})O_3$ Thin Films. *J. Phys. D: Appl. Phys.* **2011**, *44*, 105404.
54. Pantel, D.; Chu, Y.-H.; Martin, L. W.; Ramesh, R.; Hesse, D.; Alexe, M. Switching Kinetics in Epitaxial $BiFeO_3$ Thin Films. *J. Appl. Phys.* **2010**, *107*, 084111.
55. Chen, Y. C.; Lin, Q. R.; Chu, Y. H. Domain Growth Dynamics in Single-Domain-like $BiFeO_3$ Thin Films. *Appl. Phys. Lett.* **2009**, *94*, 122908.
56. Lee, W.; Han, H.; Lotnyk, A.; Schubert, M. A.; Senz, S.; Alexe, M.; Hesse, D.; Baik, S.; Gösele, U. Individually Addressable Epitaxial Ferroelectric Nanocapacitor Arrays with near Tb $inch^{-2}$ Density. *Nat. Nanotechnol.* **2008**, *3*, 402–407.